A Geometric Approach to Animating Thin Surface Features in SPH Water

Taekwon Jang
KAIST

Doyub Kim
CMU

Mi You
KAIST

Shiguang Liu
Tianjin Univ.

Junyong Noh
KAIST

Abstract

We propose a geometric approach to animating thin surface features of Smoothed Particle Hydrodynamics (SPH) based water. Explicit inter-particle connections are created among SPH particles to approximate the geometries of thin surfaces while addressing the issue of unresolved surface areas. The deformations measured on the connections actuate the animations of the surfaces by disconnecting the stretched and bent connections. The reconstruction of thin surfaces and the accuracy of the animation are improved by adding auxiliary particles over the connections via Poisson-disk sampling.

Keywords: fluid animation, inter-particle connection, smoothed particle hydrodynamics

1 Introduction

A distinctive feature exhibited by water is the existence of an interface known as a free surface. Unlike gases, water can form complex surfaces, as observed in various natural phenomena. Therefore, accurate treatment of the interface is very important to capture a realistic impression of water. Many existing studies have reproduced water surfaces faithfully [1, 2, 3]. One of the remaining challenges lies in simulating the small-scale structures of water surfaces and associated small-scale effects.

In particle fluids, surfaces are described by the composition of isovalues evaluated using individual Gaussian-like kernels defined at surface particles. Polygonal meshes are generated by applying the marching-cube method to the computed isosurfaces. As the evaluation of isovalues uses distances measured in 3D spaces, a spatial distribution of surface particles plays an important role in determining the shape and the quality of reconstructed surfaces. According to the configurations of the surface particles, the reconstructed surfaces demonstrate various appearances of liquid such as droplets, ligaments, or sheets.

A difficulty arises from the fact that a low sampling density at surfaces can lead to areas unoccupied by the kernels of particles. One remedy is to increase the number of particles adaptively at such areas. However, as the existing adaptive-sampling methods add new particles symmetrically [4], spherically [5], cubically [6], or at the corners of a tetrahedron [7] around the splittable particles, without knowledge of the target shapes to be reconstructed, the resulting sampling may differ from the thin target shapes.

In order to circumvent the issue of unresolved target geometry, we introduce explicit inter-particle connections. Specifically, we create linear connections among surface particles in sparsely sampled regions in order to approximate the unresolved geometric structures in a piece-wise manner. Conceptually, this approximation shares a similarity with nonlinear dimensionality reduction methods such as the isomap which estimates the intrinsic geometry of data,

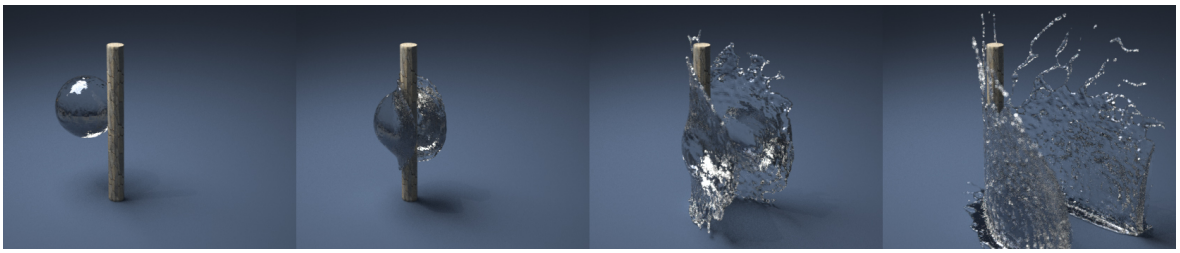

Figure 1: A sequence of images rendered from a scene with a sphere shaped water colliding with a wooden pole. The shapes and the formations of liquid sheets and liquid ligaments are captured by inter-particle connections that are created among surface particles.

based on an approximation of each data point's neighbors. Along with our inter-particle connections, we propose the following components to reproduce animations of thin surface features in Smoothed Particle Hydrodynamics (SPH) fluids.

- *Surface breakup animation method* that produces animations of thin surface features at the unresolved regions. In particular, the model determines whether the unresolved regions experience surface breakup or not, depending on the continuity status of each inter-particle connection. A linear approximation of the tensile and the bending deformations is utilized for the determination of the continuity status of each connection.

- *Dynamic upsampling method* that allows accurate checking of the continuity status of each connection by incorporating more accurate surface normals. The application of the Poisson-disk sampling method serves this purpose. Specifically, the method adds new samples to the connections to increase the sample density and improve the accuracy of the surface normals of surface particles.

- *Thin surface reconstruction method* that reconstructs surfaces including thin features by using SPH particles and inter-particle connections. We adopt a moving-average based method [8] to reconstruct smooth surfaces; in order to reproduce surfaces at unresolved areas, we extend the method by reflecting the contributions from the particles to the connections.

Our method is the first attempt to address the animation of small-scale surfaces in unresolved areas; these surfaces are difficult to handle using previous methods. As shown in Figure 1 and 2, our method allows the reconstruction and the animation of small-scale water surfaces in such regions by utilizing the inter-particle connections. In addition, our solution can be used as a post-processing tool because 1) requisite data are the geometry of particles and 2) newly generated samples during the dynamic upsampling process do not disturb the simulation results.

Inter-particle Connections The connections represent a stored set of neighbor lists of the surface particles. Here, the surface particles are the ones that have fewer than 10 neighbors. For every simulation frame, new connections can be generated for each surface particle, and the generated connections are updated or disconnected according to predefined geometric conditions. Details of the geometric conditions are given in Section 3.

2 Related Work

SPH Water Desbrun and Gascuel [9] introduced an SPH method to the computer graphics field and Müller et al. [1] extended the method to the simulation of water. Later, the method was employed in a variety of water simulations. Examples include fluid-fluid interactions [2], frothing bubbles [10], under water bubbles [11], liquid-liquid mixtures [12], porous flow [13], interfaces between multiple fluids [14], and water turbulence [15, 16]. One drawback of the SPH solver for water simulation lies in the

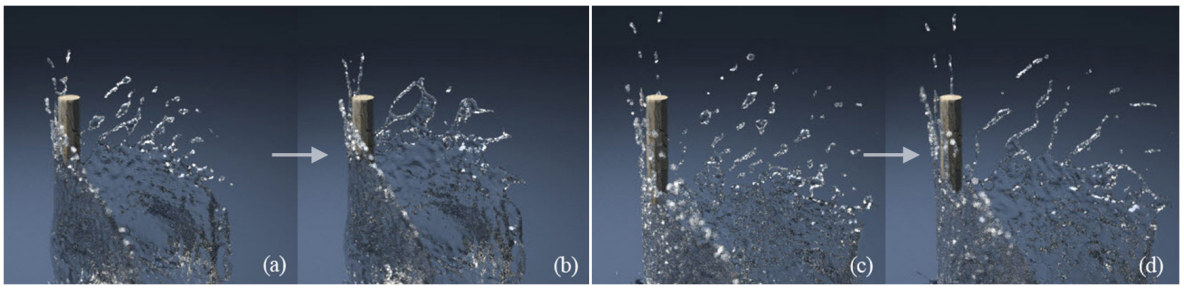

Figure 2: A sequence of images captured at (a, b) 26th frame and (c, d) 37th frame. Compared to the smooth surface reconstruction method [8], our result in (b) shows more sheets than are present in (a) and the result in (d) shows more ligaments than are present in (c).

difficulty of enforcing incompressibility due to the use of stiff equations of state (EOS). Several remedies, including a predictive-corrective incompressible SPH (PCISPH) [17], a grid-particle hybrid method [18], and the kinematic constraints based method [19] have been proposed. In addition, adaptive sampling methods [4, 6] were introduced to address the scalability issue. Recently, methods for more accurate fluid-solid coupling [20] that can incorporate the density contributions of frozen particles [3] or ghost particles [21] have been developed.

SPH Surface Reconstruction The faithful reproduction of the surfaces of SPH particles with small-scale features has been an important research topic. Solenthaler et al. [5] proposed a method to refine water surfaces via particle upsampling. Juraj et al. [22] presented a density normalization technique to address the issue of low sampling density at surfaces. For particle skinning, Bhattacharya et al. [23] proposed a constrained optimization based formulation that aims to minimize the thin-plate energy of surfaces using a level-set. In order to capture thin and continuous water surfaces, Yu and Turk [24] introduced anisotropic kernels. As the shapes of the anisotropic kernels can be transformed according to the local distribution of particles, the resultant surfaces become smoother and more stretched with fewer holes than the surfaces from the isotropic kernel [4, 8, 1]. Ando et al. [25, 26] adopted the anisotropy concept to split breakable particles in the fluid-implicit particle method (FLIP). Instead of using implicit kernels, Yu et al. [27] proposed a triangle-mesh based surface-tracking method for SPH.

3 Surface Breakup Animation

3.1 Tracking unresolved surfaces

In reality, surface breakup is a typical phenomenon that can be observed in thin water surfaces. The effects of surface tension and of high-frequency disturbances are the main physical factors that drive such a surface breakup. However, its simulation using SPH is challenging because of the existence of areas unoccupied by any particles.

In SPH water simulation, the emergence of unresolved regions can be interpreted as the result of geometric separations of the neighboring surface particles. One way to identify these separations is to trace the changes of Euclidean distance among neighboring surface particles. However, when the measurement of the inter-particle distance relies solely on a smoothing kernel, the range in which the separations can be traced is limited by the employed smoothing radius. Moreover, if one increases the radius for the tracing, measuring the distances between surface particles in every frame would require a considerable amount of computational cost due to the increase in the number of candidate neighbors.

Instead, we employ inter-particle connections between the surface particles to more efficiently track the separations across consecutive frames. The connections can reach areas that are beyond the spatial coverage of the kernels by setting the maximum connectable range larger than the ra-

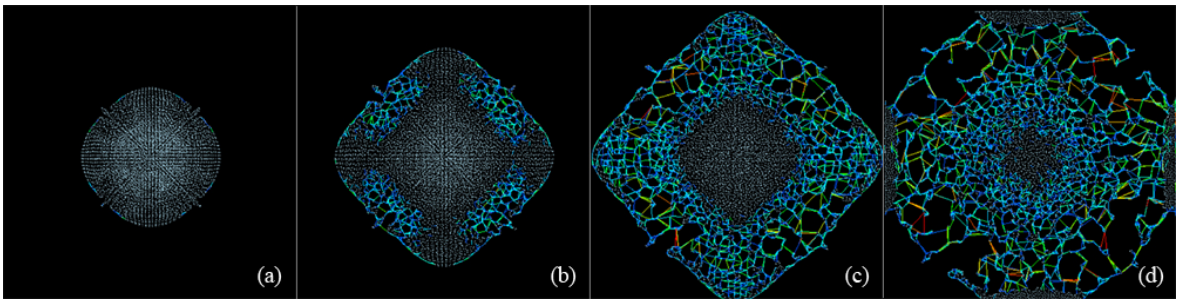

Figure 3: Visualizations of inter-particle connections. The images were captured at four simulation frames: (a) 30, (b) 40, (c) 50, and (d) 60. The connections are colored according to the magnitude of the stretching deformations from red (high) to blue (low).

dius of a kernel. The generation and disconnection of inter-particle connections are governed by several geometric conditions.

3.2 Geometric conditions for connections

Generation The directions of new connections have to be constrained to the tangential directions of the surfaces because we focus on reproducing breakable surface elements such as thin water sheets or ligaments. Consequently, the angle of a candidate vector $\mathbf{x}_{ij}$ should satisfy the following condition for the candidate to become an actual connection between a surface particle $\mathbf{x}_i$ and a neighboring surface particle $\mathbf{x}_j$.

$$|\bar{\mathbf{n}}_i \cdot \bar{\mathbf{x}}_{ij}| \leq k_t \tag{1}$$

Here, $\bar{\mathbf{n}}_i$ is the unit surface normal at $\mathbf{x}_i$, $\bar{\mathbf{x}}_{ij}$ denotes the normalized version of $\mathbf{x}_{ij}$ and k_t is set to 0.15 to validate tangential candidates. At the same time, the candidate vector has to fulfill the following distance condition since the main purpose of the connection is to properly detect the pairs of surface particles at the moment of their geometric separation.

$$d < |\mathbf{x}_{ij}| < h \tag{2}$$

Here, d represents the rest distance between particles and h is the smoothing length of the employed SPH particles. When the candidate satisfies Equations (1) and (2), it will be stored as a new connection $\mathbf{c}_{ij}$. In this way, the geometries of the unresolved areas are approximated by an aggregation of the stored connections.

Update In each simulation frame, the length of each connection is updated as the connected particles move around. Next, the connections that are either too long or too short to represent unresolved areas are removed according to the following condition.

$$|\mathbf{c}_{ij}| \leq d \quad \text{or} \quad |\mathbf{c}_{ij}| \geq h_{\max} \tag{3}$$

Here, $h_{\max}$ defines the maximum connectable range and is set to $4h$ in our experiments. In addition, a connection is removed if two connected SPH particles have more than 10 neighboring particles. This is because such particles are not surface particles and thus such connections do not represent unresolved areas anymore.

Disconnection Since thin surfaces in reality are prone to tearing and rupture by various physical factors, the simulation of surface breakup phenomenon is essential for the animation of such surfaces. In order to model the phenomenon in unresolved areas, we propose to use a geometric approach. The idea is to measure the strains of stretching deformations and the local curvatures of bending deformations over the connections; this idea is inspired by the observation that the breakup phenomena of thin sheets or thin ligaments resemble those of inextensible thin shells [28]. Thin surfaces can be torn when they experience a large stretching deformation in a short time period.

$$\frac{|\mathbf{c}_{ij}| - \left|\mathbf{c}_{ij}^p\right|}{\left|\mathbf{c}_{ij}^p\right|} \geq k_s \tag{4}$$

where $\mathbf{c}_{ij}^p$ is the length of a connection in the previous frame and k_s is set to 0.15 to capture

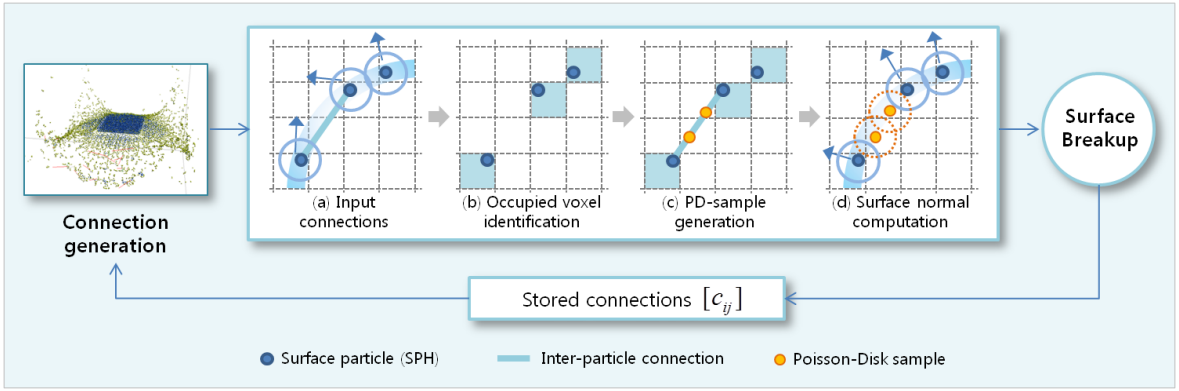

Figure 4: Our Poisson-Disk (PD) sampling technique adds a new PD sample to the inter-particle connections. These samples are then utilized at sparsely sampled regions for the computation of surface normals.

sudden stretching. In addition, we capture the breakup effect due to bending deformations by measuring the local curvature of the connection. As the curvature κ can be expressed as a divergence of unit normal $\kappa = -\nabla \cdot \bar{\mathbf{n}}$, we approximate the curvature by using the surface normal and the length of a connection as follows:

$$\frac{|\bar{\mathbf{n}}_i \cdot \bar{\mathbf{n}}_j|}{|\mathbf{c}_{ij}|} \leq k_b \tag{5}$$

where k_b is set to $(0.1/h)$. If a connection satisfies one of the two conditions for disconnection, it is removed from our system. In this way, the removal of deformed connections from a scene can approximate the breakup status of thin surface features in the unresolved areas. Figure 3 shows a visualization of the disconnections.

4 Dynamic Upsampling Method

4.1 Poisson-disk sampling method

In our system, surface normals play important roles when animating the thin surfaces. In particular, the conditions for generation and disconnection rely on the surface normals. However, it is challenging to find accurate surface normals with sparse samples. In order to increase the accuracy of the surface normals, we introduce a dynamic upsampling method. The basic idea is to provide auxiliary samples in sparse regions. Figure 4 illustrates the overall process of computing surface normals utilizing our upsampling method.

While the geometry of thin surfaces is approximated by the connections, unresolved areas suffer from deficiency of samples due to local separations of particles. In order to add more samples efficiently, we formulate the upsampling process as a Poisson-disk sampling problem because the method 1) generates and distributes samples while maintaining a minimum distance between them and 2) achieves fast performance while maintaining the sampling quality.

We adopt a fast Poisson-disk (PD) sampling technique [29] that computes upsampling with a time complexity of $O(N)$. Based on the PD sampling method, our approach skips the regions that are not occupied by any connection because such regions are not likely to be water surfaces. The next sub-section describes the procedure of our Poisson-disk sampling in detail.

4.2 Upsampling over the connections

Our upsampling process takes the inter-particle connections as input and produces auxiliary samples on the connections as output. The process begins by initializing a 3D grid that will contain both SPH particles and newly generated samples. The size of a voxel of the grid is bounded by $r/\sqrt{3}$ in order to set the minimum distance to r, which is same as the rest distance between employed SPH particles.

Step 1. Traverse the grid and mark the voxels that contain at least one SPH particle.

Step 2. Select a connection $\mathbf{c}_{ij}$.

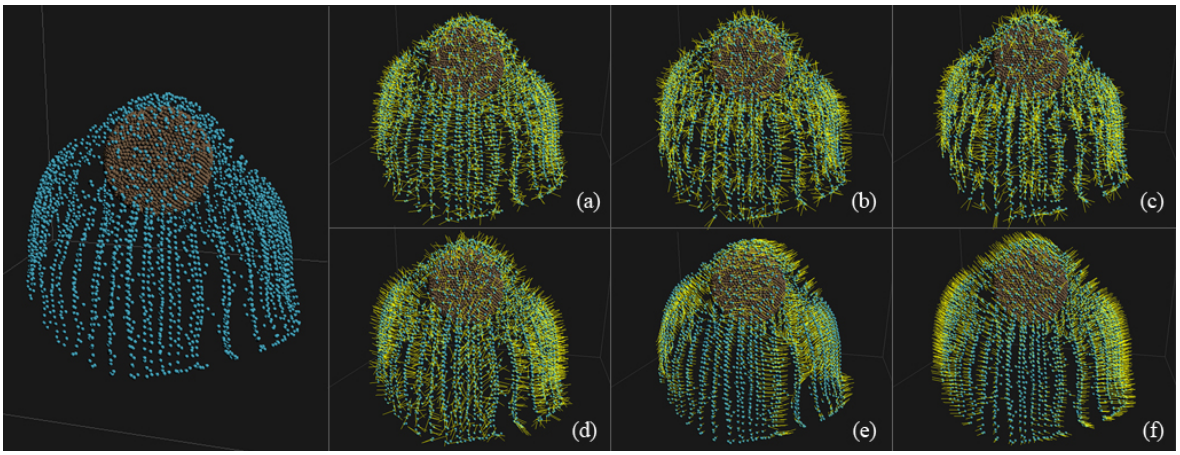

Figure 5: Comparison of normal vectors computed by (a) Color field [1], (b) Smoothed color field [14], (c) Smoothed color field, (d) Weighted PCA (WPCA) per particle, (e) WPCA per voxel, and (f) our method. The normal vectors are colored yellow. The blue particles and the brown particles represent SPH particles and a static obstacle, respectively.

Step 3. Generate candidate points in the voxels that encounter $\mathbf{c}_{ij}$.
Step 4. If the candidate point is far from existing samples or SPH particles, register the candidate point as a new sample.

In each frame, our upsampling method iterates from *Step 2* to *Step 4* while visiting all the connections. In *Step 3*, when the candidate points do not align with the connections, we move the generated samples in the direction of the normal of the connection in order to place the samples on the connection. During upsampling, we can achieve collision avoidance with existing SPH particles by treating them as pre-generated Poisson-disks. The generated PD samples maintain the minimum distance r from other samples, including the existing SPH particles.

4.3 Computing surface normals

After upsampling, we improve the accuracy of the computation of the surface normals by utilizing added PD samples. The idea is to treat the PD-samples as adjacent SPH particles when computing the mass-density and the surface normal. As the computation of SPH interpolation requires a resolved mass-density, we first compute a new mass-density for connected particles and PD samples, as follows:

$$\rho_i^* = \sum\nolimits_j m_j W_{ij} + \sum\nolimits_k m_k W_{ik} \qquad (6)$$

Here, ρ_i^* is the corrected mass-density, m_j and m_k denote the mass of an SPH particle and that of a PD sample, respectively. k is the index of nearby PD samples, and W_{ij} and W_{ik} represent a poly kernel [1] with smoothing length h.

We add the new term to the typical mass-density equation [1] to reflect the increased sampling density from neighboring PD-samples. As this correction process is applied only to the connected particles, the added term does not have any influence on other SPH particles. In addition, the corrected density field ρ^* is not incorporated into the SPH simulations, and thus the PD samples do not modify the motion of the SPH fluids. Similarly, the masses of the PD-samples m_k are also not involved in the simulation, and thus the mass-conservation of the system is not affected by this computation.

We use the color field method for the computation of surface normal vectors, as in [1]. An additional term is added to the typical equation in the same way as in the above density correction process. A normal vector for each particle can be computed as follows:

$$n_i^* = \sum\nolimits_j \frac{m_j}{\rho_j^*} \nabla W_{ij} + \sum\nolimits_k \frac{m_k}{\rho_k^*} \nabla W_{ik} \qquad (7)$$

Here, n_i^* denotes the corrected surface normal of a surface particle; ρ_j^* and ρ_k^* represent the corrected mass-density at nearby SPH particles and PD samples, respectively. By utilizing these corrected mass-densities, our method increases the

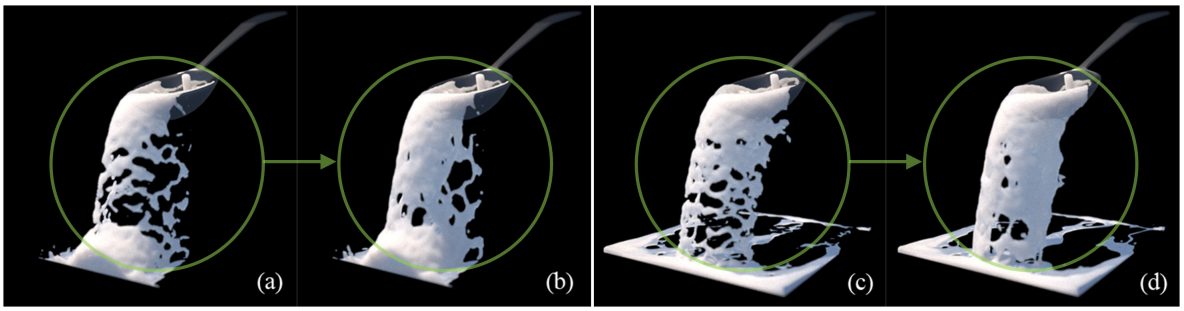

Figure 6: A sequence of images captured at (a, b) 40th frame and (c, d) 80th frame. The surfaces reconstructed using our method (b, d) have fewer holes than that underwent smooth surface reconstruction [8] (a, c) due to the contributions of the inter-particle connections at the reconstruction stage.

accuracy of the normal vectors in sparsely sampled regions. Figure 5 shows a comparison of results from our method and the existing method.

5 Thin surface reconstruction

5.1 Contributions from the connections

The breakup status of each connection, which is determined by the geometric conditions, reveals the existence of the underlying geometry in the unresolved areas. For example, when a connection is maintained, it is likely that water surfaces exist around the connection. Therefore, we reconstruct surface meshes where connections exist. Specifically, we include the contributions from the PD samples on each connection in the surface reconstruction stage.

In order to obtain smooth surfaces, we adopt a moving average based method [8] that utilizes the average position $\tilde{\mathbf{x}}$ and the average radius $\tilde{r}$. The equation for evaluating iso-values ϕ can be written as follows:

$$\phi(\mathbf{x}) = |\mathbf{x} - \tilde{\mathbf{x}}| - \tilde{r} \tag{8}$$

where $\mathbf{x}$ denotes the position of the vertex of the employed marching cube grid. Differently from the original definition, we add the contributions from the PD samples when computing $\tilde{\mathbf{x}}$ and $\tilde{r}$. Therefore, the modified equation that computes the average position can be written as follows:

$$\tilde{\mathbf{x}} = \sum\nolimits_i w_i \mathbf{x}_i + \sum\nolimits_k w_k \mathbf{x}_k \tag{9}$$

where the subscripts i and k denote the nearby SPH particles and the PD samples within the smoothing range $2h$, respectively. Similarly, the modified equation that computes the average radius can be written as follows:

$$\tilde{r} = \sum\nolimits_i w_i r + \sum\nolimits_k w_k r \tag{10}$$

where r denotes the radius of an SPH particle. w_i and w_k represent the average weights computed at each neighboring particle in the same way as in [8].

5.2 Rescaling the particle radius

When evaluating the average radius $\tilde{r}$ in Equation 10, as PD samples are additionally involved, the overall volume of the surfaces may increase. We apply the following equation in order to preserve the volume by rescaling the radius of both the SPH particles and the PD samples.

$$r = \max(r_{\min}, \sqrt[3]{n/(n+m)}r) \tag{11}$$

Here, we set $r_{\min}$ to $0.25r$ in our experiments. n and m denote the number of SPH particles and PD samples involved in evaluating the isovalues, respectively. If no PD sample is involved, r is set to be the same as the original particle radius. The effect of rescaling is valid only in the surface reconstruction stage, and does not affect the SPH simulation.

6 Results and Discussion

Implementation Our fluid solver adopts the PCISPH method [17] to enforce imcompressibility, and adopts a boundary handling method [3] for fluid-solid coupling. As the

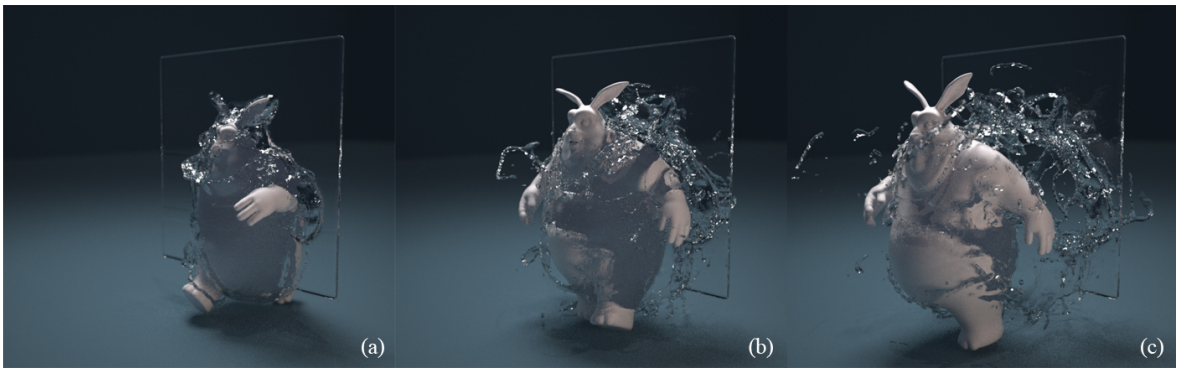

Figure 7: A space rabbit is walking across a thin water wall in a zero gravity condition. The images are from frames (a) 45, (b) 60, and (c) 75, respectively. The thin sheets over the belly of the rabbit and the thin ligaments generated from the surface breakups are captured.

simulation parameters in the geometric conditions are not sensitive to test scenes, we used fixed values in all our experiments. The surface meshes were generated by the marching cube technique with resolutions of 133x133x133 and 150x150x150 for (Cube drop/Milk Spoon scene) and (Wooden pole/Space Rabbit scene); meshes were rendered using the Maxwell renderer. Table 1 shows the average timings per simulation frame. The time spent for the marching-cube technique is also included. The process of applying the connections and upsampling consumes around the 10% of time relative to the SPH solver.

Scene name	# of particles	SPH only	Our method
Wooden pole	204,000	6.13s	6.58s
Cube drop	78,000	3.02s	3.35s
Milk spoon	120,000	4.023s	4.714s
Space rabbit	426,000	12.06s	13.174s

Table 1: Performance comparison. The simulations were performed on a system with an Intel Xeon 2.3 GHz CPU.

Fluid-object interaction Our solver samples the surfaces of objects with fluid-like particles for fluid-solid coupling. Therefore, any voxel that contains these particles is marked as occupied by Step 1 in the PD sampling process. As those voxels are skipped by Step 4, new samples are not created on the surfaces of the objects. While it is possible that new samples might be generated inside an object when parts of the connection penetrate the object, such penetrations were not observed in our experiments, such as in Figures 1, 2, 6 and 7.

Comparisons with previous work In Figures 2 and 6, the reconstruction surfaces are compared with those from Zhu and Bridson [8] in order to identify the effects of the inter-particle connections. In addition, we implemented the anisotropic kernel from Yu and Turk [24] for comparison of its effects on the surface reconstruction for filling of the unresolved areas. In Figure 8, while the anisotropic kernel [24] extends the water surfaces to the unresolved areas while the extensions are limited to the vicinity of existing particles, our results show the surfaces with fewer holes at such areas. In addition, as we add more PD samples to the sparsely sampled areas, which shares a similarity with the previous adaptive sampling methods [25, 26], we tested one scene in order to verify that our results can produce similar results in terms of preserving thin sheets. In

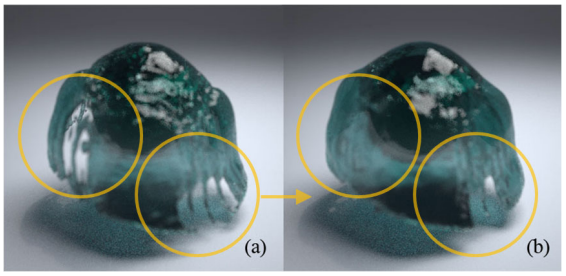

Figure 8: The surface reconstructed by (a) the anisotropic kernel [24] and (b) our method.

Figure 9, we borrowed an image from Ando et al. [26] for a side-by-side comparison. Our method produces a similar shape of thin water surface by employing several inter-particle connections.

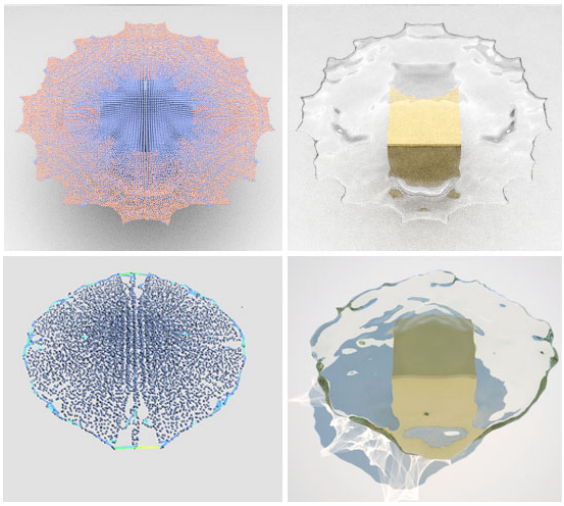

Figure 9: Images in the top-row are from Ando et al. [26]. The colored lines at the bottom-left represent the generated connections.

7 Conclusions

We presented a geometric approach to the animation of thin liquid surfaces of SPH fluids. In particular, we introduced explicit inter-particle connections that can represent the geometry of unresolved areas, allowing breakup simulation of SPH surfaces. We applied a Poisson-disk sampling method that adds PD samples to the connections for the purpose of increasing the accuracy of the breakup simulation. In addition, the PD samples were exploited in the surface reconstruction stage to reproduce thin water surfaces. We demonstrated the effectiveness of the proposed method by showing several test results.

A limitation of our method is that the animated surfaces may suffer from temporal inconsistency. Water volumes in-between particles may appear or disappear across frames resulting from the additions or deletions of PD samples to/from the connections. Such artifacts occur because the surface breakup phenomenon, which has a smooth transition phase in reality, is modeled based on a simple binary status. In future work, we will investigate a remedy that can utilize more states, such as a post-connection state and a post-disconnection state, to animate the transition smoothly, and thus to reduce artifacts.

References

[1] M. Müller, D. Charypar, and M. Gross. Particle-based fluid simulation for interactive applications. In *Proceedings of the 2003 ACM SIGGRAPH/Eurographics symposium on Computer animation*, pages 154–159.

[2] M. Müller, B. Solenthaler, R. Keiser, and M. Gross. Particle-based fluid-fluid interaction. In *Proceedings of the 2005 ACM SIGGRAPH/Eurographics symposium on Computer animation*, pages 237–244.

[3] N. Akinci, M. Ihmsen, G. Akinci, B. Solenthaler, and M. Teschner. Versatile rigid-fluid coupling for incompressible sph. *ACM Trans. Graph.*, 31(4), 2012.

[4] B. Adams, M. Pauly, R. Keiser, and L.-J. Guibas. Adaptively sampled particle fluids. *ACM Trans. Graph.*, 26(3), 2007.

[5] B. Solenthaler, Y. Zhang, and R. Pajarola. Efficient refinement of dynamic point data. In *Proceedings Eurographics/IEEE VGTC Symposium on Point-Based Graphics*, pages 65–72, 2007.

[6] B. Solenthaler and M. Gross. Two-scale particle simulation. *ACM Trans. Graph.*, 30(4), 2011.

[7] Y. Zhang, B. Solenthaler, and R. Pajarola. Adaptive sampling and rendering of fluids on the gpu. In *Proceedings Symposium on Point-Based Graphics*, pages 137–146, August 2008.

[8] Y. Zhu and R. Bridson. Animating sand as a fluid. *ACM Trans. Graph.*, 24(3), 2005.

[9] D. Mathieu and G. Marie-paule. Smoothed particles: A new paradigm for animating highly deformable bodies. In *Proceedings*

of EG Workshop on Animation and Simulation, pages 61–76. Springer-Verlag, 1996.

[10] P.-W. Cleary, S. Pyo, M. Prakash, and B. Koo. Bubbling and frothing liquids. *ACM Trans. Graph.*, 26(3), 2007.

[11] M. Ihmsen, J. Bader, G. Akinci, and M. Teschner. Animation of air bubbles with sph. In *International Conference on Computer Graphics Theory and Applications (GRAPP)*, pages 225–234. SciTePress, 2011.

[12] S. Liu, Q. Liu, and Q. Peng. Realistic simulation of mixing fluids. *Vis. Comput.*, 27(3):241–248, 2011.

[13] T. Lenaerts, B. Adams, and P. Dutré. Porous flow in particle-based fluid simulations. *ACM Trans. Graph.*, 27(3), 2008.

[14] B. Solenthaler and R. Pajarola. Density contrast sph interfaces. In *Proceedings of the 2008 ACM SIGGRAPH/Eurographics Symposium on Computer Animation*, pages 211–218.

[15] T. Jang, R.-B. Ribera, J. Bae, and J. Noh. Simulating sph fluid with multi-level vorticity. *International Journal of Virtual Reality*, 1, 2011.

[16] Z. Yuan, Y. Zhao, and F. Chen. Incorporating stochastic turbulence in particle-based fluid simulation. *Vis. Comput.*, 7:1–10, 2011.

[17] B. Solenthaler and R. Pajarola. Predictive-corrective incompressible sph. *ACM Trans. Graph.*, 28(3), 2009.

[18] K. Raveendran, C. Wojtan, and G. Turk. Hybrid smoothed particle hydrodynamics. In *Proceedings of the 2011 ACM SIGGRAPH/Eurographics Symposium on Computer Animation*, pages 33–42.

[19] K. Bodin, C. Lacoursiere, and M. Servin. Constraint fluids. *IEEE Trans. Vis. Comput. Graph.*, 18(3):516–526, 2012.

[20] B. Solenthaler, J. Schläfli, and R. Pajarola. A unified particle model for fluid–solid interactions. *Computer Animation and Virtual Worlds*, 18(1):69–82, 2007.

[21] H. Schechter and R. Bridson. Ghost sph for animating water. *ACM Trans. Graph.*, 31(4), 2012.

[22] J. Onderik, M. Chládek, and R. Ďurikovič. Sph with small scale details and improved surface reconstruction. In *Proceedings of the Spring Conference on Computer Graphics - SCCG2011*, pages 25–33, 2011.

[23] H. Bhattacharya, Y. Gao, and A. Bargteil. A level-set method for skinning animated particle data. In *Proceedings of the 2011 ACM SIGGRAPH/Eurographics Symposium on Computer Animation,*.

[24] J. Yu and G. Turk. Reconstructing surfaces of particle-based fluids using anisotropic kernels. In *Proceedings of the 2010 ACM SIGGRAPH/Eurographics Symposium on Computer Animation*, pages 217–225.

[25] R. Ando and R. Tsuruno. A particle-based method for preserving fluid sheets. In *Proceedings of the 2011 ACM SIGGRAPH/Eurographics Symposium on Computer Animation*, pages 7–16.

[26] R. Ando, N. Thurey, and R. Tsuruno. Preserving fluid sheets with adaptively sampled anisotropic particles. *IEEE Trans. Vis. Comput. Graph.*, 99(8):1202–1214, 2012.

[27] J. Yu, C. Wojtan, G. Turk, and C. Yap. Explicit mesh surfaces for particle based fluids. *Comput. Graph. Forum*, 31(2), 2012.

[28] E. Grinspun. A discrete model of thin shells. In *ACM SIGGRAPH 2006 Courses*, pages 14–19, 2006.

[29] R. Bridson. Fast poisson disk sampling in arbitrary dimensions. In *ACM SIGGRAPH 2007 sketches*.

[30] J.-P. Morris. Simulating surface tension with smoothed particle hydrodynamics. *International Journal for Numerical Methods in Fluids*, 33(3):333–353, 2000.